Ultrafast photoinduced melting of spin-Peierls phase in the organic charge-transfer compounds alkali-tetracyanoquinodimethane

K. Ikegami,[1] K. Ono,[1] J. Togo,[1] T. Wakabayashi,[1] Y. Ishige,[1] H. Matsuzaki,[1] H. Kishida,[1] and H. Okamoto[1,2,*]

[1]*Department of Advanced Materials Science, University of Tokyo, Kashiwa, Chiba 277-8561, Japan*
[2]*CREST, JST, Kawaguchi 332-0012, Japan*

Photoinduced phase transitions in spin-Peierls (SP) systems of alkali (M=K,Na)-tetracyanoquinodimethane (TCNQ) have been studied by a reflection-type femtosecond (fs) pump-probe spectroscopy. The SP phase is destabilized by the generation of photocarriers through the breaking of the spin-singlet states in dimers. It results in the decrease of the dimeric molecular displacements within a few hundred of femtoseconds over several tens of TCNQ molecules. It is accompanied by the displacive-type coherent oscillations, which consist mainly of three modes with the frequencies of 20, 49, and 90 cm^{-1} in K-TCNQ and of two modes with the frequencies of 49 and 99 cm^{-1} in Na-TCNQ. By taking into account the temperature dependence of the Raman scattering spectra, the mode with 20 cm^{-1} in K-TCNQ and the modes with 49 and 99 cm^{-1} in Na-TCNQ are assigned to the phonon modes in the SP ground state, while the modes with 49 and 90 cm^{-1} in K-TCNQ are assigned to the local modes originating from the photoexcited states. Polarization dependence of the Raman scattering signals shows that the 20-cm^{-1} mode of K-TCNQ and the 49-cm^{-1} mode of Na-TCNQ are longitudinal optical (LO) modes, whereas the 99-cm^{-1} mode of Na-TCNQ is a transverse optical (TO) mode. Namely, the LO mode plays an important role on the stabilization of the SP phase in K-TCNQ, while both the LO and TO modes in Na-TCNQ. Such a difference is discussed by scrutinizing the difference of the crystal structures and the nature of the SP transitions in the two compounds.

PACS number(s): 78.47.+p, 71.30.+h, 78.30.Jw

I. INTRODUCTION

Recent developments of the laser technology enable us to use femtosecond (fs) laser pulse in the researches for solid-state physics.[1] Among them, ultrafast control of material phases by the irradiation of a fs laser pulse is one of the most attention-gaining phenomena. This phenomenon is called photoinduced phase transition (PIPT).[2,3] The PIPT is important not only as the new subject in the fields of physics and chemistry but also as useful mechanisms for future optical switching devices. When we consider the application of PIPTs to switching devices, it is crucial to control material phases in ultrafast time scale and by small excitation photon density. A key strategy for realizing such PIPTs is the investigation of one-dimensional (1D) materials.[4–14] 1D materials have strong instability inherent to electron-lattice (EL) and/or spin-lattice (SL) interactions and sometimes show characteristic phase transitions. Therefore, if these instabilities can be controlled by photoirradiations, ultrafast PIPTs will be achieved by small excitation photon density.

In this study, we focus on the organic charge-transfer (CT) compounds, K-tetracyanoquinodimethane (TCNQ) and Na-TCNQ. The molecular structure of TCNQ is shown in Fig. 1(a). In these compounds, TCNQ molecules stack face to face as illustrated in Fig. 1(b).[15,16] An electron is transferred from an alkali metal to a TCNQ molecule and a half-filled π-electron band is formed by the overlap of the π-orbital of neighboring TCNQ$^-$ molecules. Theoretical study shows that a purely 1D electronic system with nonzero on-site Coulomb repulsion energy U has a finite gap and becomes a Mott insulator.[17] In the case of alkali(M)-TCNQ, U is large as compared to the electron transfer energy t between the adjacent molecules.[18,19] Thus, we can consider that M-TCNQ is a typical 1D Mott insulator.

K-TCNQ and Na-TCNQ undergo phase transitions at T_c =395 and 348 K, respectively.[20] Below T_c, two neighboring spins form a singlet state by alternately elongating and shrinking intermolecular distances (or equivalently molecular dimerizations) as shown in Fig. 1(c) (Refs. 15 and 16) and the system becomes diamagnetic.[21] In Figs. 2 and 3, we showed temperature dependence of the x-ray reflection intensity activated by the dimerization (open circles)[20] and of the spin susceptibility χ_p (Refs. 21 and 22) in K-TCNQ and Na-TCNQ, respectively. In K-TCNQ, with decrease of temperature from the high temperature side ($>$400 K), the x-ray reflection intensity sharply increases and χ_p sharply drops at

(a)   TCNQ

(b) Mott insulator (T>T$_c$)

M^+

TCNQ$^-$
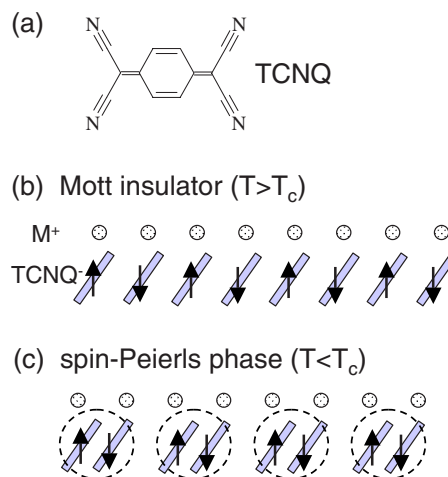
(c) spin-Peierls phase (T<T$_c$)

FIG. 1. (Color online) (a) Molecular structure of TCNQ. (b) Schematic view of the regular TCNQ$^-$ chain in the Mott insulator phase for $T>T_c$. (c) Schematic view of the dimerized TCNQ$^-$ chain in the SP phase for $T<T_c$.
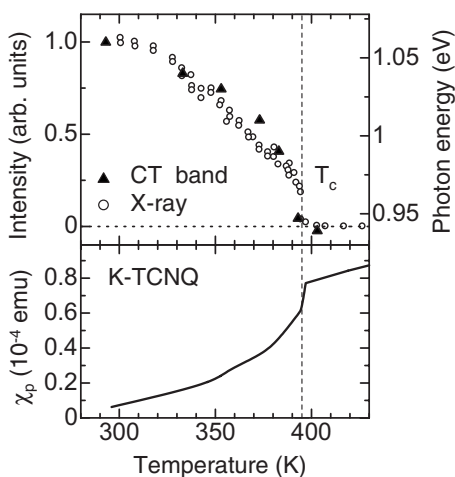
FIG. 2. Upper panel: temperature dependence of the x-ray reflection intensity (open circles) reflecting the dimeric molecular displacements (taken from Ref. 20) and the peak energy of the CT band (triangles) in K-TCNQ. Lower panel: temperature dependence of the spin susceptibility (taken from Ref. 19) in K-TCNQ.

T_c, indicating that the molecular dimerization occurs. Namely, the first-order phase transition from the paramagnetic phase to the dimerized diamagnetic phase occurs in K-TCNQ. In Na-TCNQ, the changes of the dimerization and χ_p are more continuous, although the transition of Na-TCNQ is also the first-order one.[20]

A half-filled Mott insulator with large $U (\gg t)$ can be understood as a 1D antiferromagnetic spin $(S=1/2)$ chain as shown by the arrows in Fig. 1(b). If the SL interaction exists, the molecules are dimerized at low temperatures and the neighboring two spins form a singlet state. Such a magnetic transition is called a spin-Peierls (SP) transition.[23] This transition is driven by the magnetic energy gain for the spin-singlet formation overcoming the energy loss of the dimeric lattice distortions. An SP transition is of the second-order and
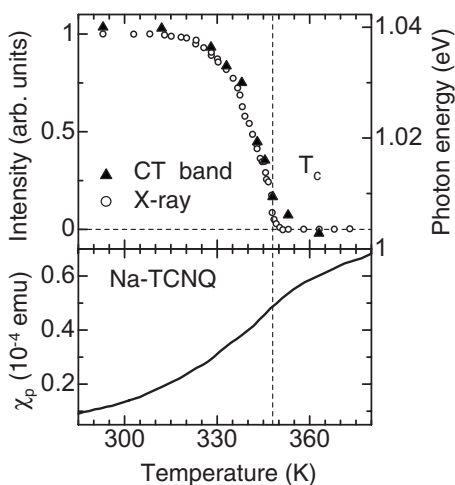

FIG. 3. Upper panel: temperature dependence of the x-ray reflection intensity (open circles) reflecting the dimeric molecular displacements (taken from Ref. 20) and the peak energy of the CT band (triangles) in Na-TCNQ. Lower panel: temperature dependence of the spin susceptibility (taken from Ref. 21) in Na-TCNQ.

the transition temperature T_p is usually very low, typically lower than 20 K.[23] The phase transitions of M-TCNQ have been regarded as a kind of SP transitions.[24–26] Actually, the phase transitions of M-TCNQ are of the first order and their transition temperatures are very high, so that they are not typical SP transitions. To explain the features of the phase transitions of M-TCNQ, the importance of the charge degree of freedom[27] and the structural nature of the transition[19] have been suggested. It is, however, reasonable to consider that the SP mechanism plays important roles on their transitions.[24–26]

In an SP phase, photocarriers will be able to stimulate the instability of the SL system through the breaking of the spin-singlet states and then the ultrafast melting of the SP phase by photoirradiation is expected to occur.[9] In fact, photoinduced destabilization of the SP phase was reported in K-TCNQ (Refs. 28 and 29) and a neutral radical crystal, trithiatriazapentalenyl (TTTA).[9]

In this paper, we report the comparative studies for the ultrafast photoinduced melting of the SP phase in K-TCNQ and Na-TCNQ using a fs pump-probe (PP) reflection spectroscopy. We found that photogenerated electrons and holes were instantaneously localized via the EL interaction, forming the polaronic states. Such polaronic carriers behaved as nonmagnetic impurities. Consequently, the SP phase was destabilized, and the dimeric molecular displacements decreased over 20–40 TCNQ molecules within a few hundred of femtoseconds. The photoinduced decrease of the dimeric molecular displacements was accompanied by the displacive-type coherent oscillations. A difference was observed in the nature of the coherent oscillations between K-TCNQ and Na-TCNQ. K-TCNQ shows three coherent oscillations (20, 49, and 90 cm^{-1}), whereas Na-TCNQ shows two (49 and 99 cm^{-1}). By comparing these coherent oscillations with the polarization dependence of the Raman scattering spectra, we have assigned the 20-cm^{-1} mode of K-TCNQ to the LO phonon mode, and the 49- and the 99-cm^{-1} mode of Na-TCNQ to the LO mode and the TO mode, respectively. All of these oscillations are inherent to the electronic ground state. The 49- and 90-cm^{-1} modes of K-TCNQ are attributable to the local oscillations associated with the photoexcited states. These results suggest that for the stabilization of the SP phase, the LO mode is important in K-TCNQ, whereas the LO and TO modes are important in Na-TCNQ. Such a difference will be discussed by scrutinizing the difference of the crystal structures and the nature of the SP transitions in the two compounds.

The contents of this paper are as follows. In Sec. II, we detail the experimental procedures. We present the experimental results and their discussions in Sec. III and IV, respectively. In Sec. V, we summarize this paper.

II. EXPERIMENTAL DETAILS

Single crystals of K-TCNQ and Na-TCNQ were grown by the liquid-phase reaction processes of constituent cations (K$^+$ and Na$^+$) and TCNQ$^-$ radical anions through diffusion in the acetonitrile solution at about 290 K.[15,16] As the starting materials for cations, commercial powders of KI and NaI were used. For TCNQ, commercial powders were purified by sev-

eral recrystalization and sublimation procedures. A typical crystal size was about $10 \times 1 \times 1$ mm^3 for K-TCNQ and $0.5 \times 0.3 \times 0.3$ mm^3 for Na-TCNQ

Polarized reflectivity spectra were measured by using a specially designed spectrometer and a Fourier transform infrared spectrometer, both of which are equipped with an optical microscope. Polarized Raman spectra were measured by using a Raman spectrometer equipped with a He-Ne laser (1.96 eV) and an optical microscope.

In the fs PP reflection spectroscopy, a Ti:sapphire (Al$_2$O$_3$) regenerative amplifier system operating at 1 kHz was employed as a light source. Output from the amplifier (800 nm: 1.55 eV) with the pulse width of 130 fs was divided into two beams. One was used for a pump light and the other was used for the excitation of an optical parametric amplifier (OPA) system. From the OPA system, the probe light pulses ranging from 0.1 to 2.5 eV were obtained. We can adjust the delay time t_d of the probe pulse relative to the pump pulse by changing the light-path length of the pump pulse. The time resolution of the apparatus is about 180 fs.

Photoconductivity (PC) measurements were conducted by placing two electrodes on the sides of a single crystal and applying dc electric field. The crystal was excited by lights from a Xe lamp monochromized through a 10-cm monochromator and modulated at a frequency of $\sim$300 Hz by an optical chopper. The applied dc eletric field and the polarization of the excitation light were set parallel to the TCNQ stacking axis (the **a** axis). The photocurrent was detected by using a lock-in amplifier. The spectral intensity of the irradiated lights was corrected by using a thermopile detector. The excitation profile of the photoconductivity was normalized to the incident photon number by taking account of the reflection loss of the incident light. Linearity of the photocurrent against the applied voltage and the intensity of the incident light were carefully checked.

III. EXPERIMENTAL RESULTS

A. Polarized reflectivity spectra

In Figs. 4(a) and 4(b), we show the polarized reflectivity (R) spectra of K-TCNQ and Na-TCNQ at 293 K for the electric field of lights E parallel ($\parallel$) and perpendicular ($\perp$) to the TCNQ stacking axis **a**. The spectra for K-TCNQ have previously been reported.[18,19] Our results in Fig. 4(a) are in good agreement with them. The spectra for Na-TCNQ have never been reported. In both K-TCNQ and Na-TCNQ, the spectra are composed of sharp structures due to intramolecular vibrational modes below 0.3 eV and broad peaks due to the electronic transitions above 0.5 eV. The main peak commonly observed at about 1 eV for $E \parallel a$ is due to the CT transition $(TCNQ^-, TCNQ^-) \rightarrow (TCNQ^{2-}, TCNQ^0)$.[18,19]

In the upper panel of Fig. 5(a), the expanded R spectrum for $E \parallel a$ (solid line) around the CT band of K-TCNQ is presented, together with the excitation-energy dependence of the photoconductivity (PC) along **a** at 77 K (open circles). The photocurrent is negligible at the CT transition peak, indicating that the lowest excited state is a CT exciton. With increasing excitation photon energy, the PC gradually increases and then is saturated at around 1.5 eV, where unbound elec-
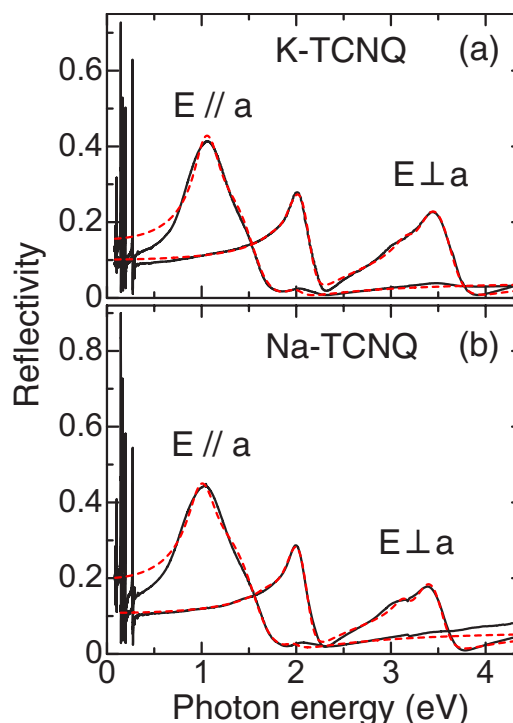

FIG. 4. (Color online) Polarized reflectivity (R) spectra (solid lines) and their fitting curves (broken lines) of K-TCNQ (a) and Na-TCNQ (b).
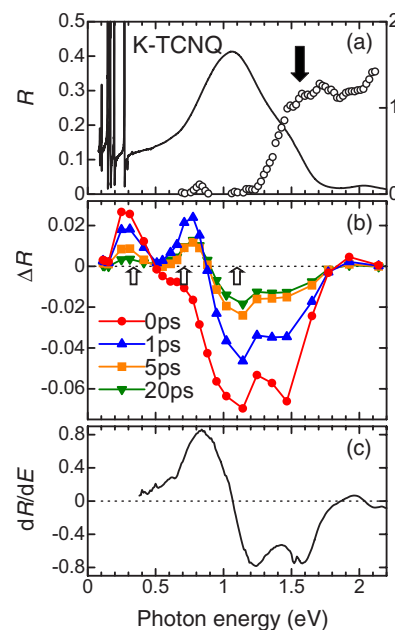

FIG. 5. (Color online) (a) Polarized reflectivity (R) spectrum for $E \parallel a$ and the excitation profile of the photocurrent along **a** (open circles) in K-TCNQ. (b) Photoinduced reflectivity changes (ΔR) spectra for the typical delay time t_d in K-TCNQ. The pump energy is 1.55 eV [the solid arrow in (a)] and the excitation density is 0.095 photon/TCNQ. Open arrows show the energy positions, at which the excitation-density dependences of $\Delta R/R$ are presented in Fig. 7. (c) dR/dE spectrum in K-TCNQ.

trons and holes are considered to be photogenerated. In Na-TCNQ, the PC measurements have not been performed because of the small size of the crystal. However, it is natural to consider that the nature of the photoexcited state in Na-TCNQ is the same as that in K-TCNQ, since the R spectra of Na-TCNQ are almost the same as those of K-TCNQ.

The shoulder structure at about 1.3 eV slightly higher than the CT peak in the R spectra of both compounds originates from the originally one-photon-forbidden CT exciton, which is activated by the dimerization through the zone folding of the exciton bands.[19] The two peak structures at around 2 and 3.4 eV observed for $E \perp \mathbf{a}$ in Fig. 4 are attributable to the intramolecular transitions or equivalently the Frenkel excitons of TCNQ. Both peaks have the shoulder structure in the low-energy side, which is also attributable to the zone-boundary excitonic states activated by the dimerization through the zone folding. It should be noted that the CT exciton with the transition dipole moment parallel to $\mathbf{a}$ has the positive dispersion of the exciton band, while the intramolecular (Frenkel) exciton with the transition dipole moment almost perpendicular to $\mathbf{a}$ has the negative one.[30] The spectra for $E \| \mathbf{a}$ show weak peaks at around 2 eV. These peaks are attributable to the leakages from the 2-eV peaks observed for $E \perp \mathbf{a}$, since the normal to the molecular planes is inclined against the $\mathbf{a}$ axis about 16° in both compounds.[15,16]

In Figs. 4(a) and 4(b), we showed the fitting curves by the broken lines by assuming a dielectric function given below

$$\widetilde{\varepsilon} = \varepsilon_\infty + \frac{Ne^2}{m_e} \sum_i \frac{f_i}{\omega_i^2 - \omega^2 - i\Gamma_i\omega},$$

$$f_i = \frac{2m_e\omega_i}{\hbar}|\langle 0|x|i\rangle|^2. \qquad (1)$$

Here, m_e, N and $\langle 0|x|i\rangle$ are the free electron mass, the number of electrons, and the transition dipole moment between the ground state and the ith excited state, whose resonance frequency and bandwidth are ω_i and Γ_i, respectively. For the spectrum for $E \| \mathbf{a}$, we assumed three oscillators; the CT exciton at around 1 eV, the shoulder structure at 1.3 eV and the small structure at 2 eV. For the spectrum for $E \perp \mathbf{a}$, we assumed four oscillators; the intramolecular transition bands at 2 and 3.4 eV, and the weak shoulder structures in their lower-energy sides. The fitting curves shown by the broken lines in Fig. 4 reproduced well the experimental spectra (the solid lines) in both compounds. The fitting parameters are presented in Table I. These parameters will be used for the comparison of the magnitudes of the Raman bands observed for different polarization configurations in Sec. IV C.

B. Photoinduced reflectivity changes

1. K-TCNQ

In Fig. 5(b), photoinduced reflectivity changes ΔR spectra ($E \| \mathbf{a}$) of K-TCNQ for 1.55-eV pump with the electric field $E_{ex} \| \mathbf{a}$ are presented for several typical delay times t_d. The excitation density was about 0.095 photon/TCNQ, which was defined by the average of the absorbed photons within the absorption depth l_p of the pump pulse and deduced by

TABLE I. Optical parameters evaluated from the analyses of the polarized reflectivity spectra by using Eq. (1) in K-TCNQ and Na-TCNQ.

K-TCNQ	parallel			perpendicular			
i	1	2	3	1	2	3	4
$\langle 0\|x\|i\rangle$ (Å)	1.31	0.852	0.239	0.240	0.992	0.464	0.619
Γ (eV)	0.204	0.562	0.215	0.184	0.215	0.223	0.330
ω (eV)	1.01	1.28	2.00	1.756	2.00	3.17	3.39
ε_∞		2.33			2.59		

Na-TCNQ	parallel			perpendicular			
i	1	2	3	1	2	3	4
$\langle 0\|x\|i\rangle$ (Å)	1.48	0.325	0.381	0.464	0.954	0.497	0.933
Γ (eV)	0.304	0.425	0.450	0.300	0.200	0.300	0.321
ω (eV)	0.859	1.39	2.10	1.76	1.97	2.99	3.37
ε_∞		1.38			2.84		

taking into account the pump-pulse density per unit area on the crystal surface, the absorption coefficient, and the reflection loss of the pump pulse.

We can discuss the ΔR spectra by dividing the measured energy region to two parts, below 0.5 eV and above 0.5 eV.
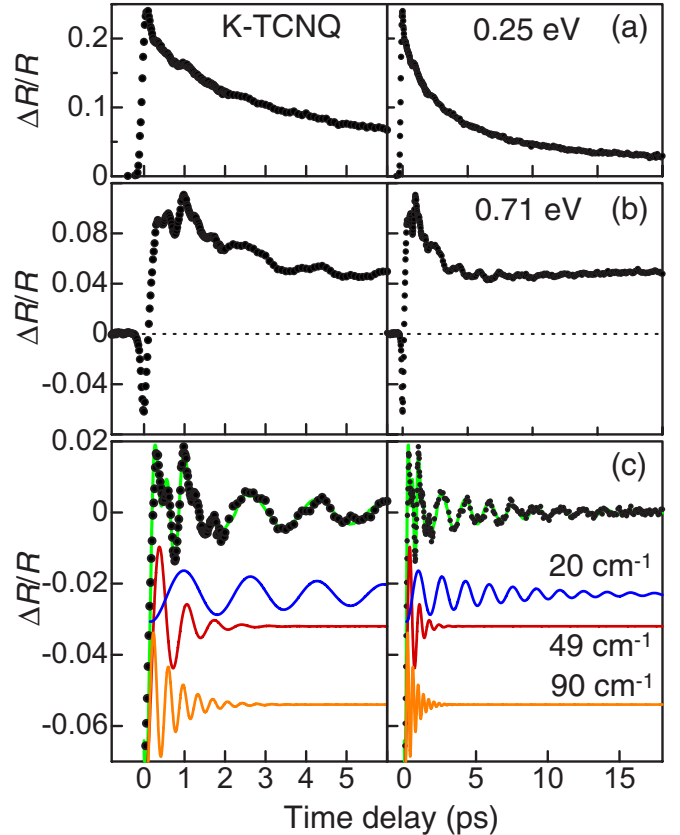

FIG. 6. (Color online) (a), (b) Time profiles of $\Delta R/R$ at (a) 0.25 eV and (b) 0.71 eV in K-TCNQ. (c) Oscillatory components (solid circles) extracted from (b). The thin solid line is a fitting curve, which is the sum of the three damped oscillators with the frequencies of 20, 49, and 90 cm⁻¹ shown in the lower region.
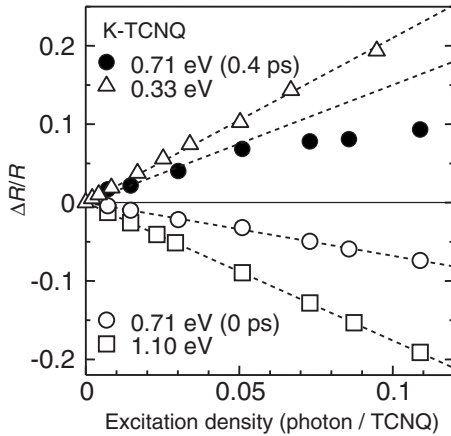
FIG. 7. Excitation-density dependence of $\Delta R/R$ at 0.33 eV (open triangles), 0.71 eV (open circles), and 1.10 eV (open squares) just after the photoirradiation ($t_d=0$ ps), and at 0.71 eV for t_d =0.4 ps (solid circles) in K-TCNQ.

Below 0.5 eV, a peak structure is observed at around 0.25 eV. Taking account of the excitation profile of the photoconductivity, the 1.55-eV excitation produces unbound electron-hole pairs, so that the observed peak is attributable to the midgap absorption originating from the localized carriers or equivalently small polarons stabilized via the EL interaction.

Figure 6(a) shows the time profile of $\Delta R/R$ at 0.25 eV, which is not a simple exponential curve. If the decay time τ_{pc} of the photocarriers is defined as the time at which the signal is equal to $1/e$ of the maximum of $\Delta R/R$, it is evaluated to be ~ 3 ps. The rise time of the midgap absorption is much less than the time resolution (~ 180 fs).

Above 0.5 eV, the ΔR spectra show characteristic spectral shapes, attributable to the spectral change of the CT band. The spectrum at $t_d=0$ ps shows that the reflectivity decreases over the whole energy region of the CT band, which is due to the bleaching of the CT band by the photoirradiation. The spectral shape after 1 ps is distinctive, especially in the region from 0.5 to 0.9 eV, in which the sign of the ΔR changes from negative to positive. The spectral shape is analogous to the first derivative of original reflectivity (dR/dE) shown in Fig. 5(c). This indicates that the photocarriers induce the redshift of the CT band within 1 ps.

In K-TCNQ, the peak energy of the CT band, E_{CT}, is strongly correlated with the degree of the dimerization. In the upper panel of Fig. 2, the temperature dependence of E_{CT} (the peak energy of the R spectrum for $E\|\mathbf{a}$) is shown by the solid triangles. E_{CT} gradually decreases with increase of temperature. The temperature dependence of E_{CT} is in agreement with that of the dimerization (open circles in Fig. 2). Such a close correlation suggests that the transient redshift of the CT band is due to the photoinduced decrease of the dimerization. Thus, the spectrum at $t_d=1$ ps indicates that the dimerization decreases by the photoirradiation within 1 ps. Namely, the ultrafast photoinduced melting of the SP phase occurs.

To clarify the dynamical aspect of the photoinduced melting of the SP phase in K-TCNQ, we show the time profile of $\Delta R/R$ at 0.71 eV in Fig. 6(b), which characterizes the redshift of the CT band and therefore reflects directly the photo-

induced decrease of the dimerization. Just after the photoirradiation, the reflectivity at 0.71 eV decreases due to the bleaching of the CT band by the photocarrier generations. In this process, the SP dimerizations will not be changed, since the periods of the lattice phonons in this type of organic molecular compounds are generally long as compared with the pulse width (~ 130 fs). Subsequently, the reflectivity sharply increases up to $t_d \sim 400$ fs due to the redshift of the CT band, which is caused by the transient decrease of the dimeric molecular displacements as mentioned above. After the delayed increase, $\Delta R/R$ decays, accompanied by the prominent oscillations. It is reasonable to consider that these oscillations are also related to the lattice phonon modes associated with the SP dimerizations. As seen in Fig. 6(b), the oscillatory components seem to consist of several modes. The period of the main oscillatory component observed even after 1 ps is about 1.6 ps. The oscillatory components will be analyzed and discussed in Sec. IV C.

The excitation density (I_{ph}) dependence of $\Delta R/R$, which is useful to estimate the efficiency of the PIPT, is presented in Fig. 7 for three typical probe energies 0.33, 0.71, and 1.10 eV, indicated by the open arrows in Fig. 5(b). $|\Delta R/R(t_d=0 \text{ ps})|$ at these energies is proportional to I_{ph} up to ~ 0.1 photon/TCNQ. In contrast, the $\Delta R/R$ ($t_d=0.4$ ps) at 0.71 eV shown by the solid circles is saturated at around $I_{ph} \sim 0.05$ photon/TCNQ. The $\Delta R/R$ ($t_d=0.4$ ps) at 0.33 eV does not show a saturation behavior but shows a linear dependence (not shown). Namely, the signal originating from the melting of the SP dimerization, is saturated at the lower excitation density than the signal originating from the generation of the photocarriers. It suggests that the melting of the SP phase is induced over a large number of molecules by the photoirradiation and a space filling occurs.

2. Na-TCNQ

The R and ΔR spectra for $E\|\mathbf{a}$ in Na-TCNQ are presented in Figs. 8(a) and 8(b), respectively. The excitation density is 0.04 photon/TCNQ. The spectral shapes of ΔR in Na-TCNQ can be understood in the similar way as in K-TCNQ; the midgap absorption located at about 0.25 eV, the photoinduced decrease of ΔR at 0.5–2 eV ($t_d=0$ ps) due to the bleaching of the CT band, and the photoinduced redshift of the CT band within 1 ps. In Na-TCNQ, the spectral shape of ΔR at $t_d=1$ ps shown in Fig. 8(b) is very similar to that of dR/dE shown in Fig. 8(c). As shown in Fig. 3, the temperature dependence of E_{CT} (the solid triangles) and the x-ray reflection intensity (the open circles) due to the dimerization are closely related with each other. From these facts, we can consider that the transient redshift of the CT band is also due to the photoinduced decrease of the dimerization, similarly to the case of K-TCNQ.

The time evolution of $\Delta R/R$ at 0.25 eV for the midgap absorption is presented in Fig. 9(a), from which the decay time of the photocarriers τ_{pc} can be evaluated to be ~ 1.8 ps. The time evolution of $\Delta R/R$ at 0.69 eV reflecting the photoinduced melting of the SP phase is shown in Fig. 9(b). We can see the initial decrease, the delayed increase and the coherent oscillations in $\Delta R/R$. Overall time profile of $\Delta R/R$ in Na-TCNQ is analogous to that of K-TCNQ except for the
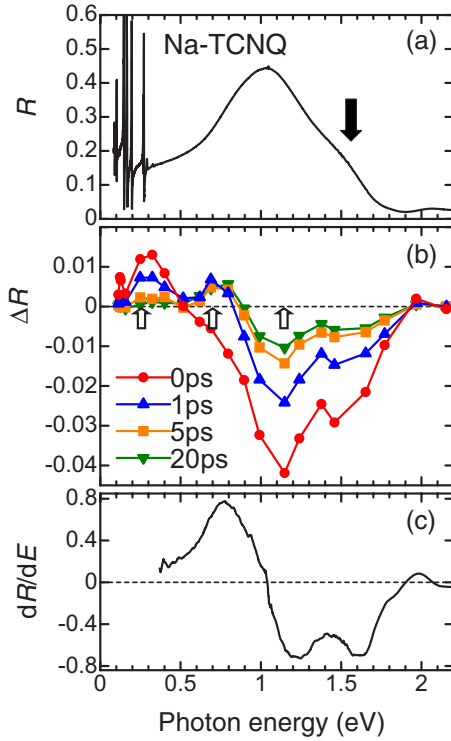
FIG. 8. (Color online) (a) Polarized reflectivity (R) spectrum for $E \parallel \mathbf{a}$ in Na-TCNQ. (b) Photoinduced reflectivity changes (ΔR) spectra for the typical delay time t_d in Na-TCNQ. The pump energy is 1.55 eV [the solid arrow in (a)] and the excitation density is 0.04 photon/TCNQ. Open arrows show the energy positions, at which the excitation-density dependences of $\Delta R/R$ are presented in Fig. 10. (c) dR/dE spectrum in Na-TCNQ.

coherent oscillations; the oscillation profile of $\Delta R/R$ in Na-TCNQ differs considerably from that in K-TCNQ.

The excitation density dependence of $\Delta R/R$ at typical probe energies is shown in Fig. 10. $|\Delta R/R(t_d=0 \text{ ps})|$ at 0.26, 0.70, and 1.14 eV, shows linear dependence on I_{ph} up to 0.1 photon/TCNQ, whereas $|\Delta R/R(t_d=0.44 \text{ ps})|$ at 0.69 eV is saturated at 0.025 photon/TCNQ. The observed features are essentially the same as those in K-TCNQ. As compared to K-TCNQ, the saturation of the $\Delta R/R$ signal reflecting the photoinduced melting of the SP phase occurs at the lower excitation photon density.

C. Polarized Raman spectra

It is natural to consider that the coherent oscillations observed on ΔR are related to the release of the dimerizations. To discuss the origins of the coherent oscillations, it is necessary to obtain information on the phonon modes associated with the dimerization. The phonon modes corresponding to the dimerization are Raman active only in the SP phase and show specific selection rules for light polarization depending on the directions of the displacements. Therefore, we measured the polarization dependence of the Raman spectra and their temperature dependence.

Raman spectra at 293 K ($<T_c$) and at 400 K ($>T_c$) of K-TCNQ are presented in Figs. 11(a) and 11(b). Here, the
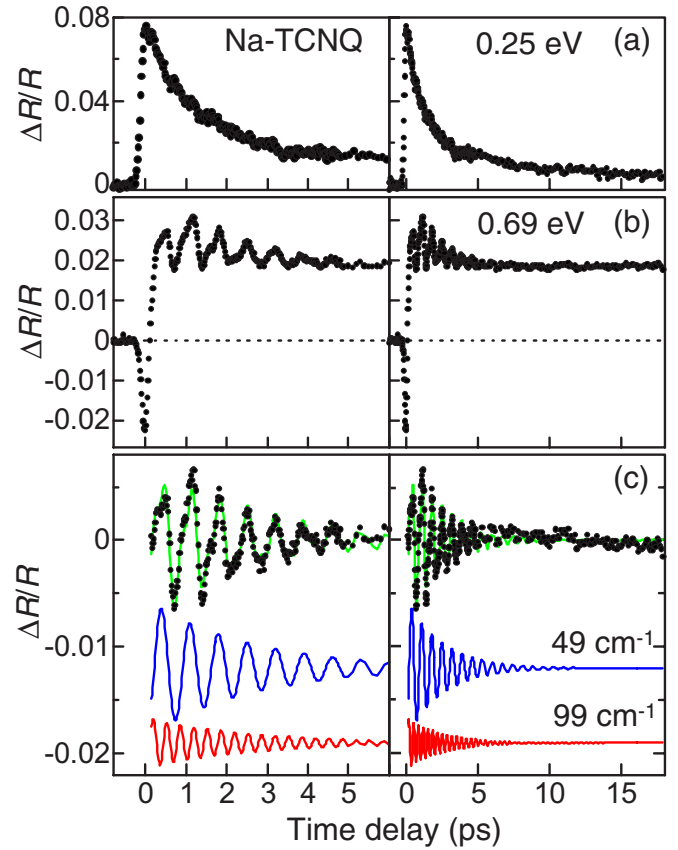

FIG. 9. (Color online) (a), (b) Time profiles of $\Delta R/R$ at (a) 0.25 eV and (b) 0.69 eV in Na-TCNQ. (c) Oscillatory components (solid circles) extracted from (b). The thin solid line is a fitting curve, which is the sum of the two damped oscillators with the frequencies of 49 and 99 cm^{-1} shown in the lower region.

polarization of the excitation light x is always parallel to the stacking axis $\mathbf{a}$ and z indicates the direction of the incident light, which is perpendicular to $\mathbf{a}$. The energy of the excitation light is 1.96 eV. The bands A–C are attributable to the zone-boundary modes in the high-T phase activated in the SP phase by the zone folding.[31] Raman spectra at 293 K
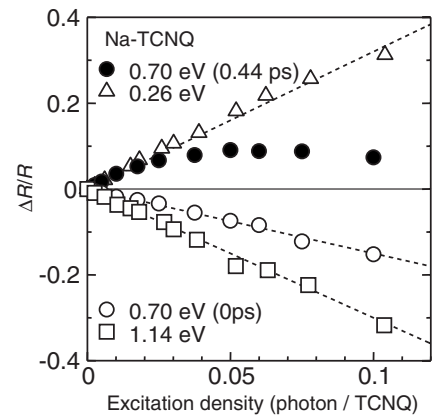

FIG. 10. Excitation-density dependence of $\Delta R/R$ at 0.26 eV (open triangles), 0.70 eV (open circles), and 1.14 eV (open squares) just after the photoirradiation ($t_d=0$ ps), and at 0.70 eV for $t_d = 0.44$ ps (solid circles) in Na-TCNQ.

FIG. 11. (Color online) Polarized Raman scattering spectra of K-TCNQ at 293 K ($<T_c$) and at 400 K ($>T_c$) for (a) $z(xx)\bar{z}$ and (b) $z(xy)\bar{z}$. The normalized spectrum for $z(xy)\bar{z}$ is shown in (c) (see text). x corresponds to the chain axis **a** and z denotes the direction of the incident light.

($<T_c$) and at 365 K ($>T_c$) of Na-TCNQ are presented in Figs. 12(a) and 12(b). The bands A′–D′ are also attributable to the zone-boundary modes in the high-T phase. These bands, A–C in K-TCNQ and A′–D′ in Na-TCNQ, will include the modes related to the SP dimerization. The comparison of the Raman bands with the coherent oscillations will be discussed in Sec. IV C.
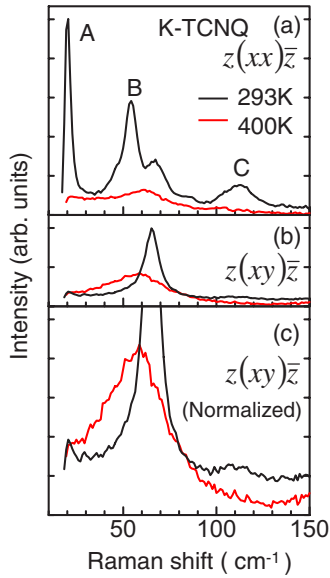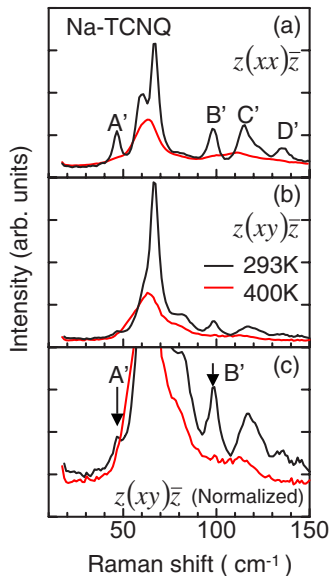

FIG. 12. (Color online) Polarized Raman scattering spectra of Na-TCNQ at 293 K ($<T_c$) and at 365 K ($>T_c$) for (a) $z(xx)\bar{z}$ and (b) $z(xy)\bar{z}$. The normalized spectrum for $z(xy)\bar{z}$ is shown in (c) (see text). x corresponds to the chain axis **a** and z denotes the direction of the incident light.
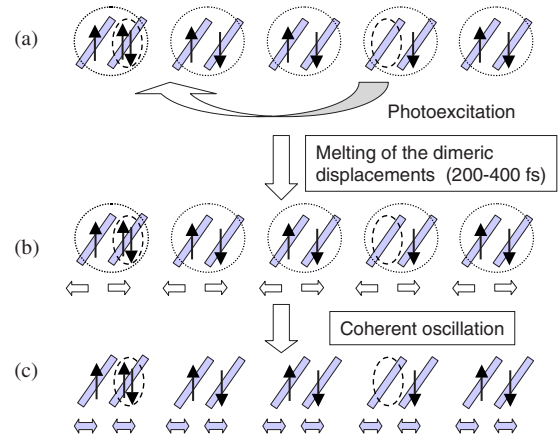

FIG. 13. (Color online) Schematic illustrations of the photoinduced melting of the SP phase; (a) the photoexcitation of an electron-hole pair, (b) the dissolution of the dimerization, and (c) the generation of the coherent oscillations.

IV. DISCUSSIONS

A. Dynamical aspects of the photoinduced melting of the SP phase

In this section, we discuss the dynamical aspects of the observed photoinduced melting of the SP phase. As mentioned in Sec. III B, the rise time of ΔR at around 0.25 eV reflecting the midgap absorption is much less than the time resolution ($\sim$180 fs) in both K-TCNQ and Na-TCNQ. Thus, the photogenerated electron and hole carriers are immediately relaxed to small polarons much faster than 180 fs. On the other hand, we can clearly detect the dynamics of the transient redshift of the CT band, the rise time τ_{rise} of which is larger than the time resolution; τ_{rise} is about 400 fs in K-TCNQ and about 200 fs in Na-TCNQ. The rise time will be related to the dynamics of the photoinduced decrease of the dimeric molecular displacements, that is, the frequency of the lattice phonons associated with the dimerization (the SP modes). These results suggest that the localization of photocarriers, that is, the small-polaron formation, should be attributed to the higher-frequency phonon modes different from the SP modes. Namely, the EL and SL interactions would be dominated by different phonon modes.

Taking these facts into account, the observed photoinduced dynamics can be explained in the following way. Photogenerated electron and hole carriers are immediately relaxed to small polarons. These polarons consist of nonmagnetic sites as schematically shown by the broken lines (ovals) in Fig. 13(a), which induce not only the breaking of the spin singlet in dimers but also the destabilization of the SP phase, since the SP phase is stabilized in an infinite spin chain. Then the polarons give rise to the release of the dimeric molecular displacements over a long range along the chain as shown in Fig. 13(b). This results in the redshift of the CT band. Such a photoinduced phenomenon is analogous to the impurity effect of the SP system, CuGeO₃, in which the SP transition is suppressed by the introduction of nonmagnetic impurities.[32] The theoretical studies also demonstrated that the magnetic-energy gain due to the SP dimerization is decreased in finite spin chains.[33]

In the time profiles of $\Delta R/R$ at 0.71 eV in K-TCNQ and at 0.69 eV in Na-TCNQ shown in Figs. 6(b) and 9(b), respectively, the prominent oscillations are observed after the delayed increase of the signals. These oscillations can be related to the release of the dimeric molecular displacements. By the photocarrier generations, the equilibrium positions of molecules should suddenly change. In this case, it is natural that the displacive-type coherent oscillations are generated. The significant result to be emphasized is that the oscillatory components are considerably different in the two compounds. The reason of the difference will be discussed in Sec. IV C later.

In K-TCNQ, the positive $\Delta R/R$ signal at 0.71 eV showing the melting of the SP phase decreases up to 5 ps and then becomes almost constant up to 20 ps, as shown in Fig. 6(b). The former decrease is attributable to the recovery of the dimerization following the decay of photocarriers with the time constant of $\tau_{pc} \sim 3$ ps. The recombination of photocarriers leads to the increase of the temperature of the SL system, which is the origin for the constant $\Delta R/R$ component, since the increase of the temperature induces a decrease of the dimeric molecular displacements and therefore the decrease of E_{CT} as shown in Fig. 2. This long-lived component decays with a time scale of microseconds. By subtracting the constant component from the time profile of $\Delta R/R$ shown in Fig. 6(b), we can see the time profile reflecting the initial recovery of the dimerization. From the residual time profile, the time constant of the initial recovery is roughly estimated to be about 3 ps, which is almost equal to τ_{pc}. This suggests that the molecular displacements recover to the initial ones just after the photocarriers recombine. The delay time of this recovery process after the recombination of carriers is very small, probably equal to τ_{rise}.

In Na-TCNQ, the magnitude of the fast recovery of the positive $\Delta R/R$ signal at 0.69 eV seems to be small as shown in Fig. 9(b). This is due to the superposition of relatively large magnitude of the bleaching signal. In order to evaluate the initial positive component in the $\Delta R/R$ signal due to the decrease of the dimerizations, it is necessary to subtract the negative component due to the bleaching from the bare $\Delta R/R$ signal. It is natural to consider that the time profile of the bleaching of the CT band is equal to that of the midgap absorption. Taking into account these facts, we can consider that the time constant of the initial recovery of the dimeric displacements is also almost equal to $\tau_{pc} \sim 1.8$ ps.

B. Efficiency of the photoinduced melting of the SP phase

In the excitation density (I_{ph}) dependence of $\Delta R/R$ in K-TCNQ (Fig. 7), $\Delta R/R$ ($t_d = 0.4$ ps) at 0.71 eV is almost linear to I_{ph} for $I_{ph} < 0.03$ photon/TCNQ, but is saturated for $I_{ph} > 0.05$ photon/TCNQ. This is in contrast to the linear I_{ph} dependence of $|\Delta R/R(t_d = 0 \text{ ps})|$ at the same energy. A possible reason for this saturation is the space filling of the domains with no or weak dimerizations induced by the photoirradiation. If the space filling is assumed to be completed for $I_{ph} = 0.05$ photon/TCNQ, the domain size destabilized by one photon is estimated to be 20 TCNQ molecules.

To evaluate the photoinduced decrease in the magnitudes of the dimeric molecular displacements, it is necessary to know the precise value of the photoinduced shift of the CT band ΔE_{CT}. By comparing $\Delta R/R$ ($t_d = 0.4$ ps)$- \Delta R/R$ ($t_d = 0$ ps) with dR/dE at 0.71 eV, we found ΔE_{CT} to be 0.04 eV for $I_{ph} = 0.05$ photon/TCNQ. The shift of the CT band between the SP phase at 293 K and the undimerized phase at 396 K is evaluated to be 0.11 eV from Fig. 2. Assuming that an excitation with $I_{ph} = 0.05$ photon/TCNQ induced the melting of the SP phase in all regions within the absorption depth, we find that the dimeric displacement is decreased to $\sim 60\%$ of the original one over 20 TCNQ per photon.

The evaluation of the efficiency for the photoinduced melting of the SP phase in Na-TCNQ can be performed in the same way. The excitation density dependence of $|\Delta R/R(t_d = 0.44 \text{ ps})|$ reflecting the photoinduced melting of the SP phase is saturated at 0.025 photon/TCNQ (see Fig. 10). Taking account of the space-filling effect, the domain size destabilized by one photon was evaluated to be 40 TCNQ molecules.

We can also estimate the magnitudes of the photoinduced decrease of the dimeric molecular displacements in Na-TCNQ. By comparing $\Delta R/R(t_d = 0.44 \text{ ps}) - \Delta R/R(t_d = 0 \text{ ps})$ with dR/dE at 0.69 eV, we obtained the ΔE_{CT} value of 0.016 eV for $I_{ph} = 0.025$ photon/TCNQ. The shift of the CT band between the SP phase at 293 K and the undimerized phase at 353 K is evaluated to be 0.034 eV from Fig. 3. Assuming that an excitation with $I_{ph} = 0.025$ photon/TCNQ induced the melting of the SP phase in all regions within the absorption depth, the dimeric molecular displacements are decreased to $\sim 70\%$ of the original one over 40 TCNQ molecules per photon. In order to obtain more precise information about the magnitudes of photoinduced changes in dimeric molecular displacements, direct observations of the structural changes by means of, for example, time-resolved x-ray diffraction studies should be necessary.

C. Analyses of the coherent oscillations

To analyze coherent oscillations observed in $\Delta R/R$ [Figs. 6(b) and 9(b)], we extracted the oscillatory components by subtracting background rise and decay from $\Delta R/R$, which are plotted by solid circles in Fig. 6(c) for K-TCNQ and Fig. 9(c) for Na-TCNQ. As shown by the thin solid lines in these figures, the oscillatory components can be well reproduced by the sum of the cosine-type damped oscillators expressed by the following formula:

$$\frac{\Delta R}{R} = \sum_i A_i \cos(\omega_i t - \phi_i) \exp(-t/\tau_i), (A_i < 0). \quad (2)$$

Each oscillatory component is also shown in the figures.

The time profile for K-TCNQ in Fig. 6(c) consists of three modes, whose frequency ω_i (decay time τ_i) is 20 cm^{-1} (5.7 ps), 49 cm^{-1} (0.53 ps), and 90 cm^{-1} (0.57 ps). The initial phase ϕ_i is almost equal to zero for each oscillation. The important feature is that the 20-cm^{-1} oscillation lives longer compared to the other two oscillations. The time profile for Na-TCNQ in Fig. 9(c) consists of two modes, whose frequency ω_i (decay time τ_i) is 49 cm^{-1} (1.9 ps) and 99 cm^{-1}

(1.9 ps). The initial phases ϕ_i are also almost equal to zero.

Here, we compare the coherent oscillations with the Raman bands activated by the dimerizations, the A–C bands in K-TCNQ and the A′–D′ bands in Na-TCNQ, as argued in Sec. III C. In K-TCNQ, the frequency (20 cm^{-1}) of the long-lived oscillation is equal to that of the band A. Therefore, the coherent oscillation can be attributed to the phonon mode of the electronic ground state in the SP state. When the dimeric displacements average out to zero after the photoirradiation, the coherent oscillation corresponds with the zone-boundary mode in the high-T phase. In this case, the frequency of the oscillatory signal on ΔR will be doubled. If anharmonicity causes the coherence of the oscillation to be lost, the oscillatory signal may disappear. The observation of the coherent oscillation with the same frequency as the Raman mode (20 cm^{-1}) indicates that the dimerization was not completely lost by the photoirradiation in our case. This is consistent with the fact that the photoinduced decrease of the dimeric molecular displacements is about 40% of the original ones as reported in the preceding subsection. The decay time (5.7 ps) of the 20-cm^{-1} oscillation is much longer than that of photocarriers $\tau_{pc} \sim 3$ ps. Namely, this oscillation survives without disturbance of the coherence even after the photocarriers decay. This fact also supports that this oscillation is due to the phonon mode of the SP ground state.

For the oscillations of 49 cm^{-1} and 90 cm^{-1}, no Raman bands are observed at the same frequencies. In addition, the decay time (~ 0.5 ps) is much shorter than τ_{pc}. Therefore, these oscillations are attributable to the local phonon modes in the photoexcited states, which are the localized photocarriers or small polarons.

In Na-TCNQ, the frequencies of the coherent oscillations (49 and 99 cm^{-1}) are equal to those of the bands A′ and B′, respectively. Therefore, these coherent oscillations can be attributed to the phonon modes of the dimerized SP ground state. The decay time of these oscillations (~ 1.9 ps) is longer than that of photocarriers τ_{pc} (~ 1.8 ps) supporting this interpretation.

Coherent oscillations related to the instabilities of the EL or SL systems induced by photoirradiations have also been reported in the insulating phase of VO$_2$,[34] the neutral and ionic phases of TTF-CA (TTF =tetrathiafulvalene and CA=p-chloranil) (Refs. 11 and 35) and the charge-order phase in (EDO-TTF)$_2$PF$_6$ (EDO-TTF =ethylenedioxytetrathiafulvalene).[12]

Next we discuss the origin of the coherent oscillations, that is, the assignment of the Raman bands A in K-TCNQ and of the Raman bands A′ and B′ in Na-TCNQ on the basis of the polarization dependence of these bands. The band A in K-TCNQ and the band A′ in Na-TCNQ are activated mainly for $z(xx)\bar{z}$ as seen in Figs. 11 and 12. The intensities for the $z(xy)\bar{z}$-polarization components of these bands are small. On the other hand, the B′ band in Na-TCNQ is observed in both the $z(xx)\bar{z}$ and $z(xy)\bar{z}$ polarizations with comparable intensities.

When we determine assignment of a Raman band from its polarization dependence of the intensity, we have to take into account magnitudes of the components in the Raman tensor $a_{\rho,\sigma}$, which is expressed with the polarizability tensor $\alpha_{\rho,\sigma}$, as follows:[36]
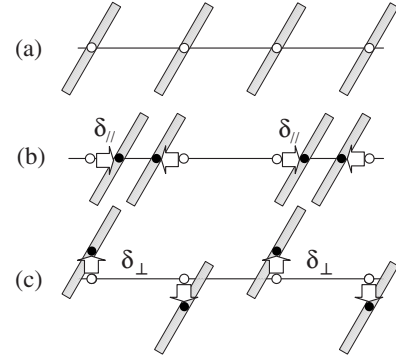

FIG. 14. (a) Schematic illustration of a regular TCNQ chain. (b) (c) Schematic illustration of dimeric molecular displacements $\delta_\parallel$ and $\delta_\perp$. The centers of molecules before and after the dimerization are shown by open and solid circles, respectively.

$$a_{\rho,\sigma} = \langle 0|\alpha_{\rho,\sigma}|1\rangle. \tag{3}$$

Here, ρ and σ denote the orthogonal coordinates. $|0\rangle$ and $|1\rangle$ are the phonon states with quantum number 0 and 1, respectively. Using the sum rule, $\alpha_{\rho,\sigma}$ can be described as follows:[36]

$$\alpha_{\rho,\sigma} = \sum_{e \neq g} \left\{ \frac{\langle g|D_\sigma|e\rangle\langle e|D_\rho|g\rangle}{h(\nu_e - \nu_g - \nu_i) - i\Gamma_e} + \frac{\langle g|D_\rho|e\rangle\langle e|D_\sigma|g\rangle}{h(\nu_e - \nu_g + \nu_i) + i\Gamma_e} \right\}. \tag{4}$$

Here, $|g\rangle$ and $|e\rangle$ show the wave functions of the electronic ground state and the electronic excited state, respectively. ν_g and ν_e are the frequencies corresponding to their energies. ν_i is the frequency of the incident photon. Γ_e is the damping constant for the electronic excited state. D_ρ and D_σ are the ρ and σ component of the dipole moment operator, respectively.

The Raman scattering intensity for the process $0 \to 1$ is determined by the square of the corresponding Raman tensor. To compare the Raman scattering intensities for different polarization configurations, therefore, it is necessary to normalize the intensities by the square of the corresponding dipole moments. By using the parameter values for the electronic transitions presented in Table I, we obtained normalized Raman spectra for $z(xy)\bar{z}$, as shown in Figs. 11(c) and 12(c), which can be directly compared with Figs. 11(a) and 12(a) for $z(xx)\bar{z}$, respectively.

The x-ray structural analyses at 298 K in K-TCNQ and 296 K in Na-TCNQ revealed that the molecular displacements exist along the molecular axis as well as along the stacking axis **a**. Since the normal to the molecular planes is slightly inclined to **a**, such a shear-type displacement, that is, the transverse optical (TO) mode, can cause the dimerization. Namely, the molecular dimerization consists of two modes, that is, the longitudinal optical (LO) mode and the TO mode, which are schematically illustrated in Figs. 14(b) and 14(c), respectively. The symmetry of the low temperature (SP) phase is C_{2h} in K-TCNQ and C_i in Na-TCNQ. Therefore, the LO mode with A_g symmetry and the TO (shear-type) mode with A_g or B_g symmetry can be detected for the $z(xx)\bar{z}$ and

TABLE II. Magnitudes of the molecular displacements parallel ($\delta_\parallel$) and perpendicular ($\delta_\perp$) to the stacking axis **a** in K-TCNQ (298 K) and Na-TCNQ (296 K) (Ref. 15 and 16). The definitions of the displacements are presented in Fig. 14.

	K-TCNQ		Na-TCNQ	
	C_1	C_2	C_1	C_2
$\delta_\parallel$(RT) (Å)	0.0876	0.0972	0.0720	0.0751
$\delta_\perp$(RT) (Å)	0.0846	0.0880	0.106	0.0717

TABLE III. Calculated intradimer transfer energy (t_1) and interdimer transfer energy (t_2) in the SP phase (298 K in K-TCNQ and 296 K in Na-TCNQ), and calculated transfer energy (t_0) for the hypothetical regular structure (see text).

		K-TCNQ		Na-TCNQ	
		C_1	C_2	C_1	C_2
SP phase at RT	t_1 (eV)	0.218	0.221	0.227	0.233
	t_2 (eV)	0.0835	0.0802	0.0893	0.102
High-T phase (hypothetical)	t_0 (eV)	0.141	0.140	0.150	0.158

$z(xy)\bar{z}$ configuration, respectively. In K-TCNQ, the band A is activated only for $z(xx)\bar{z}$, so that it can be assigned to the LO mode corresponding to the dimerization along **a**. The coherent oscillation with 20 cm^{-1} has, therefore, the same origin. In Na-TCNQ, the intensity of the band A′ for $z(xx)\bar{z}$ is much larger than that for $z(xy)\bar{z}$. Thus, it is also attributable to the LO phonon mode. The intensity of the Raman band B′ is, on the other hand, larger for $z(xy)\bar{z}$ than for $z(xx)\bar{z}$. Therefore, it is reasonable to assign the band B′ to the TO mode. Thus, the coherent oscillation with the frequency of 99 cm^{-1} is also attributable to the TO mode.

The important point we want to emphasize here is that the coherent oscillations selectively excited in the electronic ground state should be the phonon mode driving the SP transition, which is the LO phonon mode in K-TCNQ whereas the LO and TO mode in Na-TCNQ. In K-TCNQ, the TO mode may not be important so much for the stabilization of the SP phase. Such information about the phonon modes responsible for the SP instability cannot be deduced from the steady-state structural analyses using, for example, the x-ray and neutron measurements.

D. Difference in the nature of the SP transitions between K-TCNQ and Na-TCNQ

Finally, we will discuss the difference in the nature of the SP transitions and the dynamics of the photoinduced meltings of the SP phases between K-TCNQ and Na-TCNQ. First, we discuss the reason why mainly the LO mode drives the SP transition in K-TCNQ, while both the LO and TO modes drive the SP transition in Na-TCNQ. For this purpose, we scrutinize the molecular arrangements in the SP phase. In K-TCNQ and Na-TCNQ, there are two TCNQ stacking columns C_1 and C_2, which have slightly different molecular arrangements. We denote the magnitudes of the molecular displacements parallel and perpendicular to **a** as $\delta_\parallel$ and $\delta_\perp$, respectively. The definitions of the parameters are illustrated in Fig. 14. Here, $\delta_\parallel$ and $\delta_\perp$ at room temperature (at 298 K for K-TCNQ and at 296 K for Na-TCNQ) are denoted by $\delta_\parallel$(RT) and $\delta_\perp$(RT), respectively. These values are presented in Table II.[15,16] In K-TCNQ, the difference in the magnitudes of $\delta_\parallel$(RT) [$\delta_\perp$(RT)] between C_1 and C_2 is small. The difference in the magnitudes of $\delta_\parallel$(RT) [$\delta_\perp$(RT)] between the two compounds is also not so large. Therefore, it is difficult to deduce the reason for the difference of the phonon modes driving the SP instability directly from Table II.

The SP instability is caused by the phonon mode, which modulates the exchange energy J. Since J is expressed as $4t^2/U$ when $t \ll U$, the degree of the modulation in t by a molecular displacement determines the magnitude of the SL interaction. Since the molecular positions at RT in the crystals were obtained by the x-ray structural analyses, we can calculate the intradimer (t_1) and interdimer (t_2) transfer energy by using the extended Hückel method.[37] The calculated t_1 and t_2 are listed in Table III. In addition, we calculated the transfer energy in the case that the molecules are regularly arranged. In this calculation, the lattice constants at room temperature are fixed and the hypothetical molecular positions with no dimeric molecular displacements are used. The obtained values of the transfer energies (t_0) are also listed in Table III. The difference of t_0 between the columns C_1 and C_2 is small for the regular stacking structures in both compounds. Next, we evaluated how J was modified depending on the changes of the dimeric molecular displacements. For the measure of the modulation of J by the dimeric molecular displacements, we use the parameter $\Delta = (t_1^2 - t_2^2)/2t_0^2$. Here, we changed $\delta_\parallel$ from 0 to $\delta_\parallel$(RT) with $\delta_\perp = 0$ or changed $\delta_\perp$ from 0 to $\delta_\perp$(RT) with $\delta_\parallel = 0$. The obtained results are presented in Fig. 15. The magnitudes of Δ by the molecular displacements ($\delta_\parallel$) parallel to **a** in K-TCNQ and Na-TCNQ are almost the same with each other as shown in Fig. 15(a),
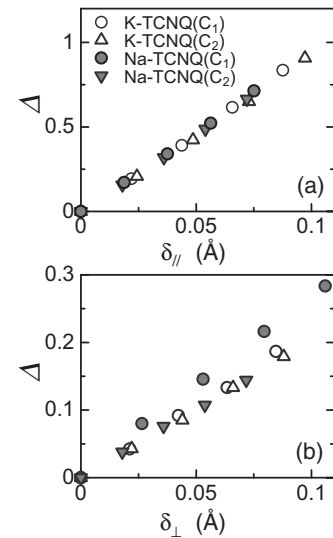

FIG. 15. Dependence of Δ on the dimeric molecular displacements, $\delta_\parallel$ and $\delta_\perp$; (a) $\delta_\parallel$ dependence of Δ for $\delta_\perp = 0$ and (b) $\delta_\perp$ depencence of Δ for $\delta_\parallel = 0$. C_1 and C_2 denote the column 1 and the column 2, respectively.

while the magnitudes of Δ by the molecular displacements ($\delta_\perp$) perpendicular to **a** are larger for the C_1 column in Na-TCNQ than in K-TCNQ [Fig. 15(b)]. These results suggest that the SL interaction for the TO mode is relatively large in the C_1 column of Na-TCNQ and the observed coherent oscillation with the frequency of 99 cm^{-1} might be attributed to the TO mode with the shear-type displacements in the C_1 column. The difference of Δ between the two compounds is, however, not so large, making us expect the presence of other reason for the difference in the nature of the phase transition including the role of the TO mode.

As mentioned in Sec. I, the phase transitions of M-TCNQ are not typical SP transitions. Especially, the transition of K-TCNQ is of the strong first-order, suggesting that it would include nature of a structural phase transition. If we take into account structural nature of the transition, a following scenario may be possible; when the molecular displacements along **a** are introduced through the SP mechanism in K-TCNQ, the occurrence of the molecular displacements perpendicular to **a** may decrease the total energy of the system through the gain of the 3D electrostatic energy or lattice energy. In this case, the first-order phase transition will occur, accompanied with the dimeric molecular displacements both parallel and perpendicular to **a**. In Na-TCNQ, the transition is more continuous. It is, therefore, natural to consider that the structural nature of the transition is small and the phase transition is dominated mainly by the SP mechanism. Namely, the TO mode will also induce the SP instability as well as the LO mode. As detailed in Sec. IV B, the photoinduced melting of the SP phase occurs over 20 molecules per photon in K-TCNQ and over 40 molecules per photon in

Na-TCNQ. This might also be explained by the strong SP nature in the transition of Na-TCNQ.

V. SUMMARY

Photoinduced melting of the spin-Peierls phase has been investigated in K-TCNQ and Na-TCNQ by the femtosecond pump-probe reflection spectroscopy. Transient reflectivity changes below 0.5 eV show a photogeneration of a midgap absorption due to the small polarons stabilized by the electron-lattice interaction. Analyses of the transient reflectivity changes at $0.5-2$ eV suggest that the dimeric molecular displacements decrease over $\sim$20 TCNQ molecules for K-TCNQ and $\sim$40 for Na-TCNQ within a few hundred of femtoseconds, reflecting collective nature of the SP systems. Such a melting of the SP phase drives the coherent oscillations of cosine type; three modes (20, 49, and 90 cm^{-1}) were observed for K-TCNQ, and two modes (49 and 99 cm^{-1}) for Na-TCNQ. By comparing the coherent oscillations with the temperature dependence of the Raman scattering spectra, the mode of 20 cm^{-1} in K-TCNQ and the two modes (49 and 99 cm^{-1}) in Na-TCNQ are assigned to the phonon modes in the electronic ground state. Polarization dependence of the Raman bands indicates that the 20-cm^{-1} mode of K-TCNQ and the 49-cm^{-1} mode of Na-TCNQ are LO modes whereas the 99-cm^{-1} mode of Na-TCNQ is a TO mode. The observed differences of the transition behaviors were discussed by taking into account the differences about the spin-Peierls nature and the structural nature of the transitions in the two compounds.

---

*okamotoh@k.u-tokyo.ac.jp

[1] For example, *Ultrafast Phenomena XIV*, edited by T. Kobayashi *et al.*, Vol. 79 of Springer series in Chemical Physics (Springer, Berlin, 2005).

[2] *Photoinduced Phase Transitions*, edited by K. Nasu (World Scientific, Singapore, 2004).

[3] Special topics "*Photo-Induced Phase Transitions and their Dynamics*," J. Phys. Soc. Jpn. **75**, 011001 (2006).

[4] S. Iwai and H. Okamoto, J. Phys. Soc. Jpn. **75**, 11007 (2006).

[5] S. Koshihara, Y. Tokura, T. Mitani, G. Saito, and T. Koda, Phys. Rev. B **42**, 6853 (1990).

[6] S. Koshihara, Y. Tokura, K. Takeda, and T. Koda, Phys. Rev. Lett. **68**, 1148 (1992).

[7] S. Iwai, S. Tanaka, K. Fujinuma, H. Kishida, H. Okamoto, and Y. Tokura, Phys. Rev. Lett. **88**, 057402 (2002).

[8] H. Matsuzaki, T. Matsuoka, H. Kishida, K. Takizawa, H. Miyasaka, K. Sugiura, M. Yamashita, and H. Okamoto, Phys. Rev. Lett. **90**, 046401 (2003).

[9] H. Matsuzaki, W. Fujita, K. Awaga, and H. Okamoto, Phys. Rev. Lett. **91**, 017403 (2003).

[10] S. Iwai, M. Ono, A. Maeda, H. Matsuzaki, H. Kishida, H. Okamoto, and Y. Tokura, Phys. Rev. Lett. **91**, 057401 (2003).

[11] H. Okamoto, Y. Ishige, S. Tanaka, H. Kishida, S. Iwai, and Y. Tokura, Phys. Rev. B **70**, 165202 (2004).

[12] M. Chollet, L. Guerin, N. Uchida, S. Fukaya, H. Shimoda, T. Ishikawa, K. Matsuda, T. Hasegawa, A. Ota, H. Yamochi, G. Saito, R. Tazaki, S. Adachi, and S. Koshihara, Science **307**, 86 (2005).

[13] H. Matsuzaki, M. Yamashita, and H. Okamoto, J. Phys. Soc. Jpn. **75**, 123701 (2006).

[14] H. Okamoto, H. Matsuzaki, T. Wakabayashi, Y. Takahashi, and T. Hasegawa, Phys. Rev. Lett. **98**, 037401 (2007).

[15] M. Konno and Y. Saito, Acta Crystallogr., Sect. B: Struct. Crystallogr. Cryst. Chem. **B30**, 1294 (1974).

[16] M. Konno, T. Ishii, and Y. Saito, Acta Crystallogr., Sect. B: Struct. Crystallogr. Cryst. Chem. **B33**, 763 (1977).

[17] E. H. Lieb and F. Y. Wu, Phys. Rev. Lett. **20**, 1445 (1968).

[18] K. Yakushi, T. Kusaka, and H. Kuroda, Chem. Phys. Lett. **68**, 139 (1979).

[19] H. Okamoto, Y. Tokura, and T. Koda, Phys. Rev. B **36**, 3858 (1987).

[20] H. Terauchi, Phys. Rev. B **17**, 2446 (1978).

[21] J. G. Vegter and J. Kommandeur, Mol. Cryst. Liq. Cryst. **30**, 11 (1975).

[22] J. G. Vegter and J. Kommandeur, Chem. Phys. Lett. **3**, 427 (1969).

[23] J. W. Bray, L. V. Interrante, I. S. Jacobs, and J. S. Miller, in *Extended Linear Chain Compounds*, edited by J. S. Miller (Plenum, New York, 1983), Vol. 3, p. 353.

[24] Y. Lepine, A. Caille, and V. Larochelle, Phys. Rev. B **18**, 3585

(1978).

[25] Y. Takaoka and K. Motizuki, J. Phys. Soc. Jpn. **47**, 1752 (1979).

[26] Y. Lepine, Phys. Rev. B **28**, 2659 (1983).

[27] S. A. Bewick and Z. G. Soos, J. Phys. Chem. B **110**, 18748 (2006).

[28] S. Koshihara, Y. Tokura, Y. Iwasa, and T. Koda, Phys. Rev. B **44**, 431 (1991).

[29] H. Okamoto, K. Ikegami, T. Wakabayashi, Y. Ishige, J. Togo, H. Kishida, and H. Matsuzaki, Phys. Rev. Lett. **96**, 037405 (2006).

[30] M. Pope and C. E. Swenberg, in *Electronic Processes of Organic Crystals and Polymers*, 2nd ed. (Oxford University Press, Oxford, 1999).

[31] M. Yoshikawa, S. Nakashima, A. Wada, and A. Mitsuishi, J. Phys. Soc. Jpn. **55**, 1177 (1986).

[32] M. Hase, I. Terasaki, Y. Sasago, K. Uchinokura, and H. Obara, Phys. Rev. Lett. **71**, 4059 (1993).

[33] D. Guo, T. Kennedy, and S. Mazumdar, Phys. Rev. B **41**, 9592 (1990).

[34] A. Cavalleri, Th. Dekorsy, H. H. W. Chong, J. C. Kieffer, and R. W. Schoenlein, Phys. Rev. B **70**, 161102(R) (2004).

[35] S. Iwai, Y. Ishige, S. Tanaka, Y. Okimoto, Y. Tokura, and H. Okamoto, Phys. Rev. Lett. **96**, 057403 (2006).

[36] G. Placzek, *Handbuch der Radiologie* (Akademische Verlagsgesellschaft, Leipzig, 1934), Vol. VI, Teil II.

[37] T. Mori, A. Kobayashi, Y. Sasaki, H. Kobayashi, G. Saito, and H. Inokuchi, Bull. Chem. Soc. Jpn. **57**, 627 (1984).